# RESEARCH ARTICLE

Journal of Optics and Photonics Research 2025, Vol. 2(4) 212–221

DOI: 10.47852/bonviewJOPR52024061



# Study of the Effects of Compositional Constituents on the Physical Properties of Inorganic Halide Perovskite Thin Films Prepared via Spin-Coating Deposition Method

S. Jalil<sup>1</sup>, Ghulam Hasnain Tariq<sup>1,\*</sup>, S. Yaseen<sup>1</sup>, Sana Ullah<sup>2</sup>, Muhammad Ijaz Khan<sup>2</sup> and Ghulam Asghar<sup>3</sup>

Abstract: Inorganic perovskite materials, for their high absorption coefficient, become attractive candidates for solar cell applications. Increasing efficiency of perovskite solar cell (PSC) devices increased attention to the launch of novel device configurations with these materials. Halide perovskite materials including CsPbIBr<sub>2</sub> demonstrate exceptional electro-optical and structural properties. In the present work, we provided a novel framework for the fabrication of CsPbIBr<sub>2</sub> thin films with physical properties sufficient for photovoltaic applications. Halide species play a crucial role in controlling the stability and efficiency of these devices. The CsPbIBr<sub>2</sub> thin films were prepared to study the effect of halide ions concentration on their physical properties. Thin films were deposited by spin-coating method with increasing concentrations of lead bromide in CsPbIBr<sub>2</sub> precursor solutions, and, after the deposition, the films were annealed at 120 °C. The prepared thin films were then characterized for conductivity type, structural, and optical properties for application in solar cell devices. X-ray diffraction (XRD) characterizations showed polycrystalline nature of thin films with diffraction peaks appearing at 15.2° and 30.4° for (100) and (200) planes. UV-VIS spectroscopy showed small variations in optical band gaps with varying precursor concentrations. Fourier transform infrared (FTIR) analysis revealed the presence of C-H, C=C, N-H, and COO functional groups in prepared thin films. Hot-probe technique applied to determine conductivity type revealed stable intrinsic nature with no boosted variation. The obtained results on the physical properties of CsPbIBr<sub>2</sub> thin films indicated that they are better candidates for photovoltaic applications. The work also presents a facile new approach to prepare cost-effective, environment friendly, and highly efficient CsPbIBr<sub>2</sub> PSC devices.

Keywords: inorganic perovskites, spin-coating, hot-probe method, solar cell, halide perovskites

#### 1. Introduction

Human population increases, and, along with industrial growth, the demand for clean energy is increasing in parallel. Environmental problems and limited availability of conventional fossil fuel energy sources are serious concerns. Therefore, consistent alternative renewable energy sources are much needed to replace fossil fuels or at least contribute to their lesser use. The use of these alternative energy sources also contributes to environmental issues related to fossil fuels. Different technologies, procedures, and systems [1–3] are being proposed to enhance efficiency of alternative energy resources. Similarly, different techniques are presented to improve performance of in-use alternative energy devices using allied layers [4], environment-friendly ingredients [5],

hybrid systems [6], and double-layered anodes [7] in available technologies. Thermoelectric technologies offer yet another alternative energy resource [8]. However, among the available alternate energy sources, solar energy is a capable alternate source as it is unlimited and provides pollutants-free environment. Solar energy could be utilized in different applications by converting it into the other forms of energy, especially into electricity by using solar cell devices. Among the different types of solar cells, perovskite-based solar cell devices are becoming promising light-harvesting structures owing to their superiorities of high light absorption coefficient and defect tolerance, low exciton binding energy, as well as long carrier lifetime and diffusion length [9].

Perovskite solar cells (PSCs) have great prospects as one of the leading next-generation photovoltaic devices because of the breakthrough in their power conversion efficiency from the initial 3.8% to more than 25.2% lately over a decade. These breakthrough efficiencies are mainly because of unique optoelectronic properties, such as large absorption coefficients,

<sup>&</sup>lt;sup>1</sup>Institute of Physics, Khwaja Fareed University of Engineering and Information Technology, Pakistan

<sup>&</sup>lt;sup>2</sup>Institute of Mechanical and Manufacturing Engineering, Khwaja Fareed University of Engineering and Information Technology, Pakistan

<sup>&</sup>lt;sup>3</sup>Department of Physics, The University of Poonch, Pakistan

<sup>\*</sup>Corresponding author: Ghulam Hasnain Tariq, Institute of Physics, Khwaja Fareed University of Engineering and Information Technology, Pakistan. Email: hasnain.tariq@kfueit.edu.pk

<sup>©</sup> The Author(s) 2025. Published by BON VIEW PUBLISHING PTE. LTD. This is an open access article under the CC BY License (https://creativecommons.org/licenses/by/4.0/).

high defect tolerant ability, tunable band gap, long photoexcited carrier lifetime, etc. There, however, remain some concerns about severe hysteresis loss and poor long-term stability impeding largescale commercial applications of PSCs [10]. All the inorganic perovskites, CsPbBr<sub>3</sub>, CsPbIBr<sub>2</sub>, CsPbI<sub>2</sub>Br, and CsPbI<sub>3</sub> have their advantages and disadvantages [11, 12]. For example, CsPbBr<sub>3</sub> may have the best stability but the wide bandgap of 2.36 eV is too large for the efficient light absorption [13]. Although the band gap of CsPbI<sub>2</sub>Br, and CsPbI<sub>3</sub> is around 1.8 eV, beneficial to the light absorption and PSC, the narrow band gap delivers poor stability [14, 15]. All these limitations in the characteristics of described perovskites restrain their applications in inorganic PSC devices. CsPbIBr<sub>2</sub> thin films have a band gap that varies from 2.20 eV to 2.24 eV. Among these perovskites, CsPbIBr<sub>2</sub> might be better choice in comparison to others in the application of inorganic PSCs [12] to balance the high efficiency and good stability. This work, therefore, is focused on the preparation of CsPbIBr2 perovskite material and its characterization for application in PSC devices.

Among the perovskite materials, halide perovskites containing halogen ions, i.e., bromide (Br-), chloride (Cl-), or iodide (I-) are of utmost importance in optoelectronic devices. CsPbI2Br and CsPbI<sub>3</sub> are extraordinary semiconducting materials for the use in optoelectronic detectors in layer form [16]. The optoelectronic perovskite materials like CsPbIBr<sub>2</sub> have optimum band gap energies and limited binding energy of excitons [17]. Because of the characteristics, halide-based perovskite materials are identified as the materials with reliable applications in optoelectronic and photovoltaic devices. Halide perovskite inorganic or mixed inorganic & organic materials are more interesting due to their optimum physical properties. Various deposition methods were employed to prepare thin films of perovskite material, such as chemical vapor deposition [18], spray deposition [19], ambient deposition [20], RF magnetron sputtering [21], solution processing [22], blade coating [23], one-step solution deposition [24, 25], and electrodeposition [26], chemical bath deposition [27], dip-coating [28, 29] and thermal evaporation [30]. The PSC devices are an extension of dye-sensitized solar cells [31].

To the best of our knowledge, there was no detailed work available on the study of physical properties of CsPbIBr<sub>2</sub> thin films subjected to annealing effects on physical properties. In the present work, thin films of halide perovskite materials were deposited by a single-step deposition with the help of spin-coating technique. The prepared CsPbIBr2 thin films were annealed at 120°C to consistently improve their structure. The structure of thin films determines all of their physical properties associated with their applications in solar cell devices. The CsPbIBr<sub>2</sub> thin films were prepared to accomplish optimal physical properties for their lightabsorbing applications in devices. The achieved physical properties emphatically support CsPbIBr<sub>2</sub> thin films suitable as light-absorbing layer for PSCs. The obtained physical properties emphatically indicate that the CsPbIBr<sub>2</sub> thin films are suitable as light-absorbing layer in PSCs. The thin films can be used for hybrid photovoltaic devices [32] for optimizing their applications to mitigate energy needs and enhance renewable energy usage. Also, the photovoltaic solar energy can be used for pumping water [33] instead of fossil fuels.

# 2. Materials and Methods

In this work,  $CsPbIBr_2$  thin films were prepared by spin-coating and annealed at  $120^{\circ}C$  for 30 min to render uniform structure of the prepared thin films. The precursor solutions to spin-coat  $CsPbIBr_2$  thin films were prepared with increasing concentration of lead bromide ( $PbBr_2$ ) in  $CsPbIBr_2$ . Four different precursor solutions

Table 1
Concentration scheme of precursors for CsPbIBr<sub>2</sub> thin films' preparation

Sample	CsI	PbBr <sub>2</sub>
S1	250 mg	250 mg
S2	250 mg	300 mg
S3	250 mg	350 mg
S4	250 mg	400 mg

were prepared wherein PbBr<sub>2</sub> concentration was varied while concentration of cesium iodide (CsI) was kept same. Then thin films were deposited on well-cleaned glass substrates by spin-coating. The precursors were prepared by using PbBr<sub>2</sub> and CsI as primary ingredients. All the ingredient materials, including dimethyl sulfoxide (DMSO), isopropanol (IPA), and acetone, were purchased from Sigma-Aldrich in Pakistan. Distilled water prepared by Millipore water purification system (Model: ELIX 3S KIT (IL), France) was used as the solvent and in cleaning solutions employed in the fabrication of CsPbIBr<sub>2</sub> thin films. Thin films were deposited on microscopic glass slides. A 250 mg CsI concentration solution along with 250 mg PbBr<sub>2</sub> concentration solution was dissolved in 1 ml DMSO solution under constant magnetic stirring at 50°C For the other precursors, CsI concentration remained same while concentration of PbBr<sub>2</sub> was varied, as given in Table 1.

# 2.1. Substrate cleaning

The cleaning of the substrate is important to obtain contamination-free deposition of the thin films. A contamination-free well-cleaned substrates provide good adhesion for the deposited thin films, and, before spin-coating of the thin film materials, the cleaning process of glass substrates was: (1) 5 min with a cleaning detergent, and (2) washed in a flow of distilled water, then (3) substrates were put subsequently in acctone and IPA for 10 and 5 min (4) in final step substrates were dried at 60°C and kept in air-tight container till deposition of thin films.

## 2.2. Preparation of thin films

The spin-coating deposition of the perovskite light-absorbing layers was carried in nitrogen environment. The deposited  $CsPbIBr_2$  thin films were kept in ambient to dry for 5 min, and, then, annealing of these thin films was done at  $120^{\circ}C$  for 20 min to reach better structural characteristics in these thin films and to improve their optoelectric properties. The films were kept in an airtight box until characterization of their physical properties. Figure 1 shows the schematic representation of the experimental procedure adopted for the preparation of thin films. The images of the thin films, as they appear after annealing at  $120^{\circ}C$ , are shown in Figure 2.

#### 2.3. Characterizations of thin films

The deposited thin films were characterized for electric and optical properties to determine their suitability for application in perovskite-based thin film solar cell devices. X-ray diffraction analysis was carried out to study different structural parameters, including crystallite size, crystalline nature, and micro-strains of CsPbIBr $_2$  thin films in the diffraction angle scan range of  $20-60^\circ$ . Transmission data were acquired by using an UV-Visible spectrometer (BK-D560) for the wavelengths ranging from 400 to 600 nm. Transmission data were used to calculate different optical

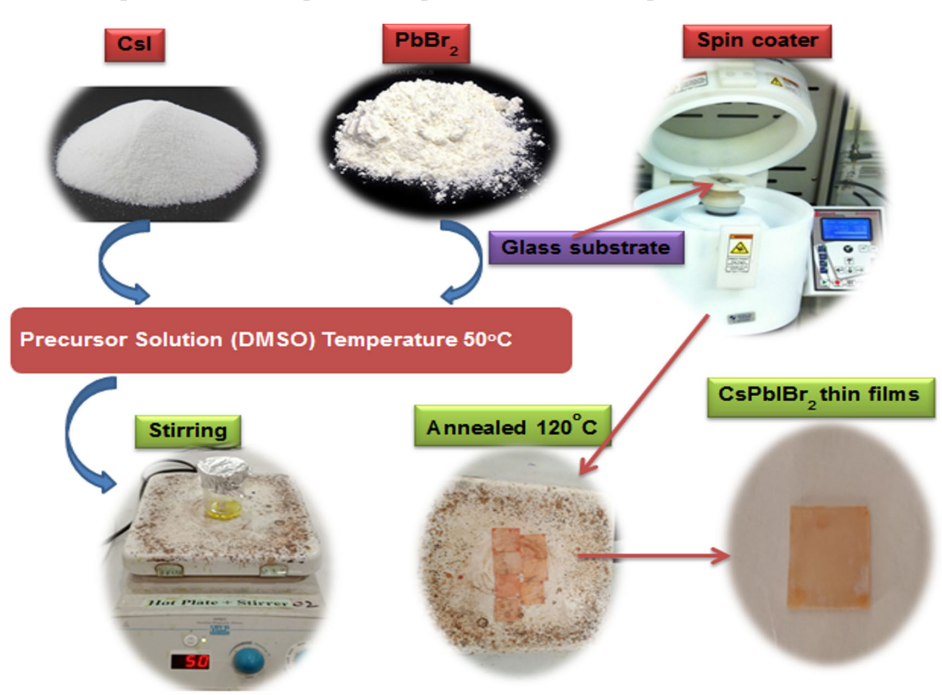
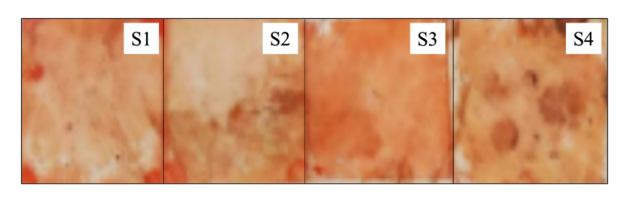


Figure 1
Schematic representation of experimental procedure used for deposition of CsPbIBr<sub>2</sub> thin films

Figure 2
Photographic images of the CsPbIBr<sub>2</sub> thin films after annealing



parameters, such as absorption coefficient and band gap energy. With the help of an Fourier transform infrared spectrophotometer (Agilent Cary 630), the occurrence of functional groups on the surface of the manipulated thin film was detected in transmittance mode between 4000 and 500 cm<sup>-1</sup>. Conductivity type of prepared CsPbIBr<sub>2</sub> thin films was determined by hot-probe method. The gravimetric weight different method was used to estimate thickness of CsPbIBr<sub>2</sub> thin films [34, 35].

## 3. Results and Discussion

Halide perovskite thin films were characterized for structural and electro-optical properties and the results are detailed below along with discussions.

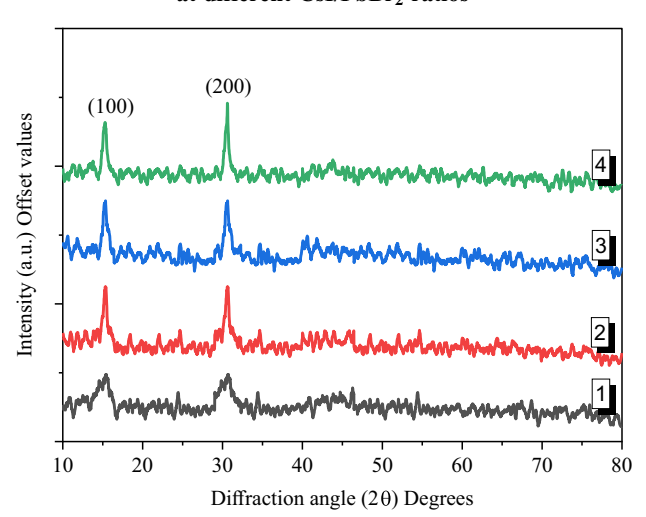
# 3.1. XRD structural analysis

Crystalline structure of prepared  $CsPbIBr_2$  thin films was observed by XRD technique. In Figure 3 are the XRD patterns recorded for  $CsPbIBr_2$  thin films with the  $CsI:PbBr_2$  ratios equal to 1:1 (S1), 1:1.2 (S2), 1:1.4 (S3), and 1:1.6 (S4).

The XRD patterns showed polycrystalline nature with two strong diffraction peaks appearing at 15.2, and 30.4°. The peaks

Figure 3

XRD spectra of CsPbIBr<sub>2</sub> thin films prepared at different CsI/PbBr<sub>2</sub> ratios



represent (100) and (200) crystallographic planes, respectively, and are well matched with the literature [36–38]. This higher peak intensity indicates that the prepared CsPbIBr<sub>2</sub> thin films have a tendency of vertical plane growth, which is favorable for transport of charges [12, 39]. The fabricated thin films show the presence of pure CsPbIBr<sub>2</sub> phase any noticeable impurity peaks, elemental or compound, revealing that increase in PbBr<sub>2</sub> concentration can stimulate the growth of this phase and improve crystallinity of the films without producing any additional phase and/or causing structural changes. Full width at half maximum (FWHM) of all of CsPbIBr<sub>2</sub> thin films with varied CsI:PbBr<sub>2</sub> ratios was calculated

Figure 4
Fitting peaks for FWHM of a CsPbIBr<sub>2</sub> thin film prepared with CsI:PbBr<sub>2</sub> = 1:1

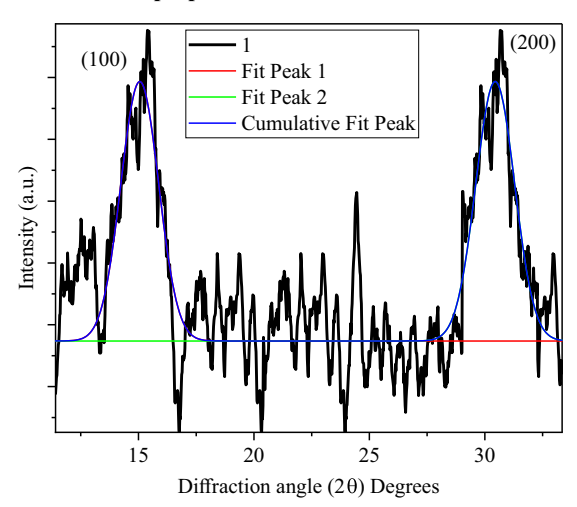
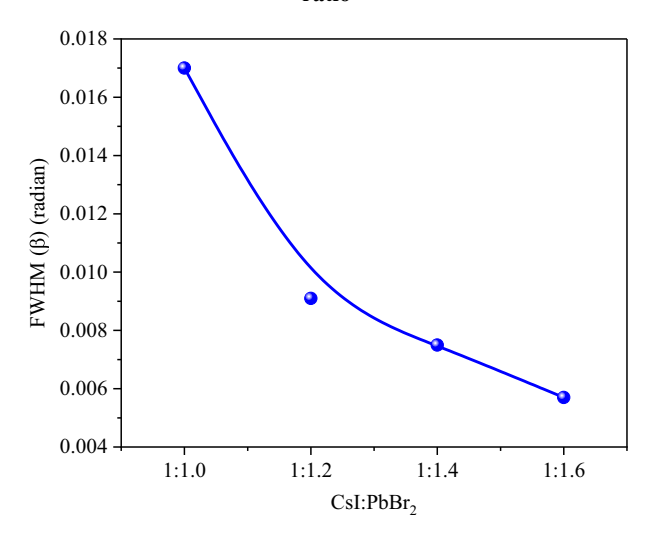


Figure 5
FWHM of the CsPbIBr<sub>2</sub> thin films as a function of CsI:PbBr<sub>2</sub>
ratio



by using Origin-2021 software. Gaussian model was used for finding of FWHM (w) values by fitting the experimental and cumulative fit peaks. A representative obtained fitting plot for FWHM of  $CsPbIBr_2$  thin films prepared with  $CsI:PbBr_2=1:1$  is shown in Figure 4.

The obtained FWHM values for all prepared CsPbIBr<sub>2</sub> thin films with different CsI:PbBr<sub>2</sub> ratios are shown in Figure 5 and are presented in Table 2. The crystallite size (D) is estimated from the Scherer formula, Equation (1):

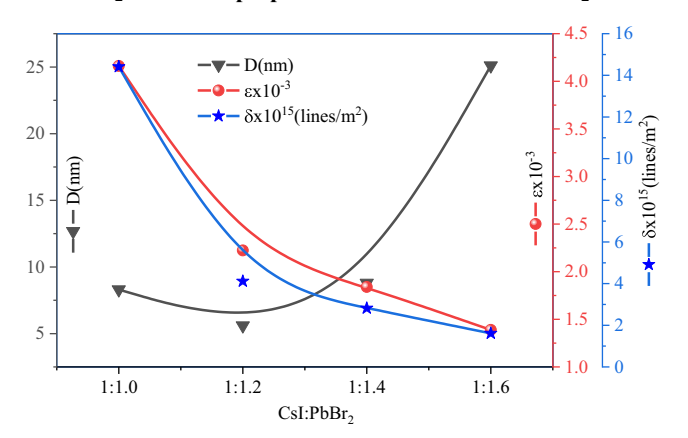
$$D = \frac{k\lambda}{\beta Cos\theta} \tag{1}$$

where D, k,  $\beta$ ,  $\theta$ , and  $\lambda$  are the crystallite size, Scherrer constant, FWHM, angle of diffraction, and X-ray wavelength, respectively. The micro-strain is calculated using the following Equation (2) [40]:

Table 2
Structural parameters calculated from XRD data of CsPbIBr<sub>2</sub> thin films

	CsI:PbBr <sub>2</sub>	FWHM			$\delta \times 10^{15}$
Sample	ratio	(rad)	D (nm)	$\varepsilon \times 10^{-3}$	(lines/m <sup>2</sup> )
S1	1:1.0	0.0170	8.3	4.1614	14.4126
S2	1:1.2	0.0091	5.6	2.2234	4.1153
S3	1:1.4	0.0075	8.8	1.8404	2.8192
S4	1:1.6	0.0057	25.1	1.3890	1.6099

Figure 6
Crystallite size, micro-strain, and dislocation density of
CsPbIBr<sub>2</sub> thin films prepared with different CsI:PbBr<sub>2</sub> values



$$\varepsilon = \frac{\beta Cos\theta}{4} \tag{2}$$

Dislocation density could be calculated by using Williamson and Hall (W-H) method [41] and Williamson and Smallman (W-S) relation. In the present work, it was investigated using W-S Equation (3) [42]:

$$\delta = \frac{1}{D^2} \tag{3}$$

The calculated values of different structural parameters are given in Table 2 and are also plotted in Figure 6. These results revealed crystal growth with increase in PbBr<sub>2</sub> concentration and a decrease in micro-strain and dislocation density.

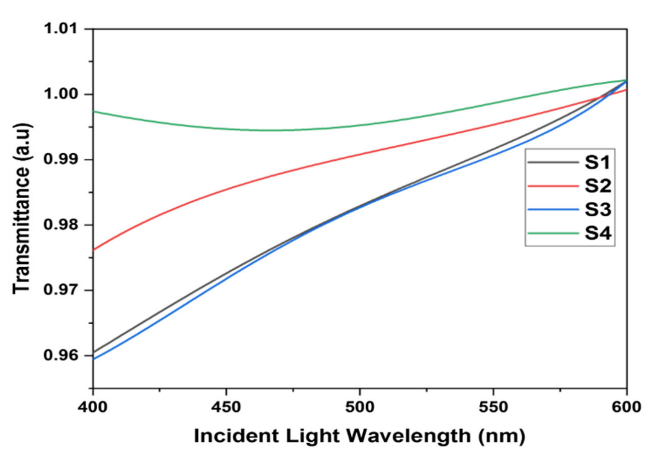
### 3.2. Optical analysis

Optical properties of thin films are most important because solar cells are photovoltaic devices. Absorption of light and its conversion into electricity by solar cells depends upon their optical response. Transmission data help in obtaining the optical parameters of prepared thin films for light absorption according to their band gap energy and absorption coefficient. These properties were calculated from transmission data.

## 3.2.1. Transmission of incident light

The thin film transmittance and absorption are important properties determining its efficiency in a solar cell. The absorption  $\alpha$  and extinction k coefficients rely on the different concentrations of PbBr<sub>2</sub> in deposited thin films. Charge carrier band-to-band

Figure 7
Transmittance spectra of CsPbIBr<sub>2</sub> thin films annealed 120°C



transitions could explain the changes in extinction coefficient at different light energies. Transmission spectra of the CsPbIBr $_2$  thin films prepared for different concentrations and annealed at 120°C are presented in Figure 7.

#### 3.2.2. Absorption of incident light

Absorption spectroscopy analysis in the range from ultraviolet to visible in the light spectrum provides absorption characteristics of the target thin films. The absorption spectra presented in Figure 8 show that absorption is higher at shorter wavelengths.

Absorption coefficient was determined by the following relation using the transmission data:

$$\alpha = -\frac{1}{t} \ln \frac{1}{T} \tag{4}$$

In this relation, t is the film thickness and T is the transmittance. The absorbance of incident light by  $CsPbIBr_2$  thin films with different concentrations of  $PbBr_2$  is presented in Figure 8. As seen in Figure 8, the samples annealed at  $120^{\circ}C$  with varied concentrations have higher absorption and can be utilized more efficiently, and the

Figure 8
Absorbance of incident light by CsPbIBr<sub>2</sub> thin films with different concentrations of PbBr<sub>2</sub>

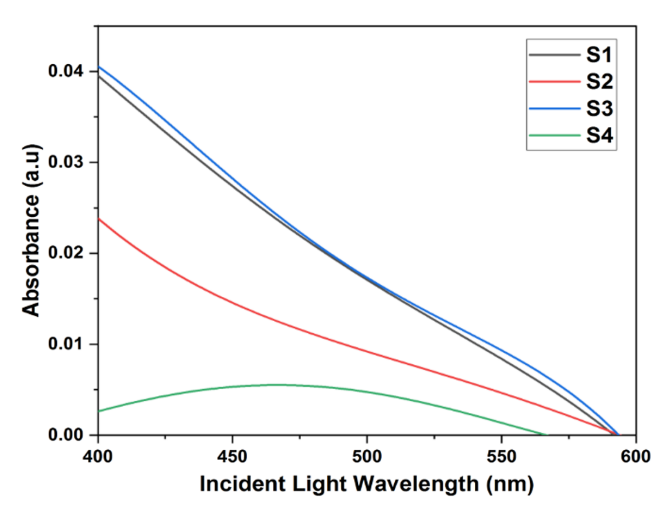
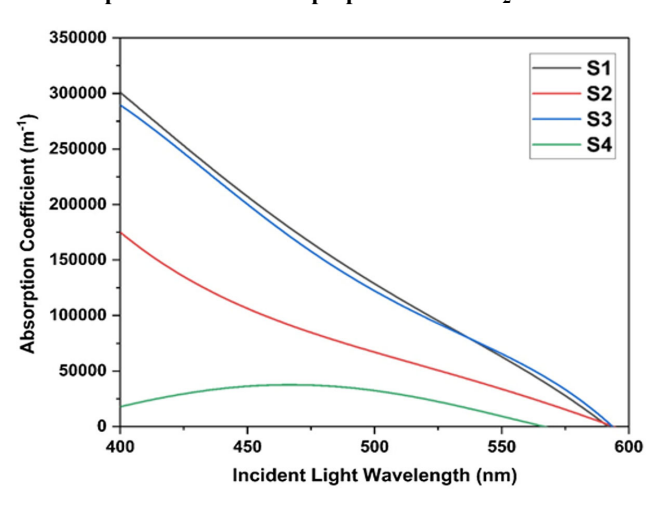


Figure 9
Absorption coefficients of prepared CsPbIBr<sub>2</sub> thin films



absorption by  $CsPbIBr_2$  thin films as a function of wavelength decreases as the wavelength increases. Figure 9 presents the dependance of absorption coefficient on incident light wavelength and reveals that how far light of a particular wavelength can penetrate into a material before it is absorbed.

#### 3.2.3. Extinction coefficient of thin films

In optical measurements, extinction coefficient and its determination are crucial. An effective and efficient optical system can be prepared if the optical response of absorbing material is well known. The absorption length of incident light in light-absorbing layer could be governed by extinction coefficient. In the present work, the value of extinction coefficient is determined by Equation (5):

$$k = \frac{\alpha \lambda}{4\pi} \tag{5}$$

where  $\alpha$  is the absorption coefficient and  $\lambda$  is the wavelength (nm) of incident light ranging from 400 to 600 nm. Behavior of thin films to incident light wavelengths for absorption coefficient is presented in Figure 10.

The reduction in extinction coefficient with the incident light wavelength increase represents the light loss on absorption. For CsPbIBr<sub>2</sub> thin films, the extinction coefficient k increases with increasing CsI concentration, as shown in Figure 9, and it indicates the effect of post-deposition annealing of these thin films. The absorption and extinction coefficients are larger for incident light with  $\lambda = 400$  nm, and, then, these coefficients fall and gradually diminish.

## 3.2.4. Optical density

To determine the optical density (OD) of  $CsPbIBr_2$  thin film utilizing transmission data, the following relation (Equation (6)) was used to compute the medium transmittance at a particular wavelength:

$$OD = log_{10} \frac{1}{T} \tag{6}$$

where T is the light transmission. Figure 11 is the relation between OD and incident light showing how OD changes with incident light wavelength ( $\lambda$ ). OD follows the same pattern as the absorption coefficient, and this trend indicates that CsPbIBr<sub>2</sub> thin films are

Figure 10
Dispersive extinction coefficients of the CsPbIBr<sub>2</sub> thin films

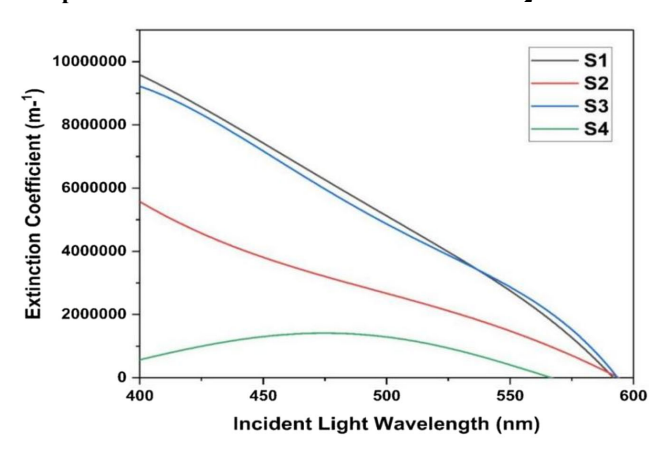
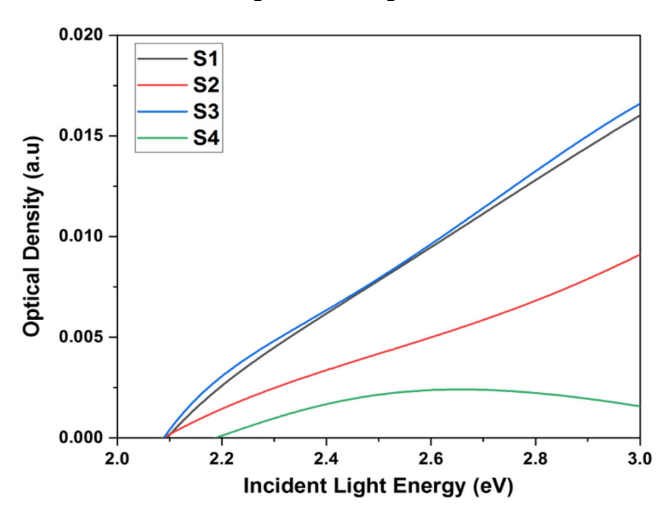


Figure 11
Dependence of optical density on different concentrations
of PbBr<sub>2</sub> in CsPbIBr<sub>2</sub> thin films

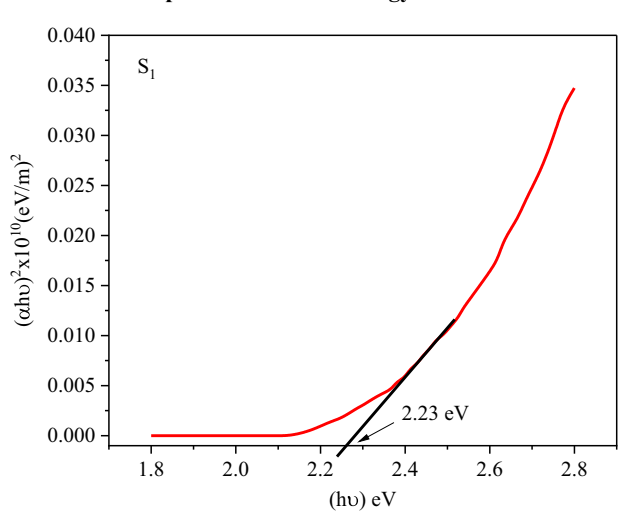


becoming more efficient in absorbing light as concentration of  $PbBr_2$  increases in the precursors.

## 3.2.5. Band gap energy

For optoelectronic applications, a critical parameter of material is its band gap energy  $E_g$ . It controls the quantity of light energy of solar spectrum absorbed by the photovoltaic cell. Calculations of  $E_{\sigma}$ for all constituent layers of a solar cell device are important. The lower  $E_g$  value may be attributed to the allowed energy state in the band gap energy during film production, while the higher  $E_g$ value can be linked to the exceptional fine grain size of thin film. Halide perovskite materials have optimal band gap energy to harvest the most intensive part of solar energy spectrum. The band gap of ABX<sub>3</sub> perovskite thin films S1, S2, S3, S4 can be changed from 2.23 to 2.21, 2.20, 2.24 eV, respectively, by mixing or exchanging halogens ions (X = Cl, Br, and I) or cations (B = Pb, Ge, and Sn). Halide perovskite semiconductors have direct band gap and significant absorption peaks. By varying the film composition, there is a minor variation in the absorption coefficient. The energy gap controls the absorption of light in the material for a specific incoming wavelength. With the use of the

Figure 12
Plot of  $(\alpha h v)^2$  vs (hv) and extrapolated its linear part towards the energy axis



Tauc relation, as given by Equation (7), the band gap energy  $(E_g)$  of CsPbIBr<sub>2</sub> thin films was determined:

$$(\alpha h \nu) = B(h \nu - E_{g})^{n} \tag{7}$$

In this relation, h is the Plank constant,  $\alpha$  is the absorption coefficient, n is the constant number, and v is the incident light frequency. The relationship between  $(\alpha h \upsilon)^2$  and incident light energy (h $\upsilon$ ) is linear after absorption edge in case of electron-to-electron direct transfer (n = 1/2) or for  $(\alpha h \upsilon)^2 = B(h \upsilon - E_g)$  [43–45]. In present study, the Tauc relation was used with  $n = \frac{1}{2}$  for CsPbIBr<sub>2</sub> thin films to find their band gap energy. This analysis confirmed that the electrons in the CsPbIBr2 thin films exhibited a direct transition, as for various concentrations plot have a straight transition in absorption region. The dependance of  $(\alpha h \nu)^2$  against the incident light energy (h $\nu$ ) was plotted and extrapolated linear portion of plot to the x-axis, where x-intercept provides band gap energy value  $(E_g)$ , which is displayed in Figure 12. By extending the linear absorption of plot to the x-axis, where the absorption coefficient is zero ( $\alpha = 0$ ), we have  $h\nu = E_g$ . A blue shift is seen for the absorption edge and it is related to a rise in energy of band gap through increasing the PbBr<sub>2</sub> concentration in thin films. The measured values of the band gap lied at 2.23, 2.21, 2.20, and 2.24 eV for CsPbIBr<sub>2</sub> thin films annealed at 120°C. This might be attributed to structural variations in the deposited CsPbIBr2 thin films due to annealing. The obtained band gap energies for varied PbBr2 concentration in prepared thin films are reported in Table 3, and it illustrates that, with increasing concentration of PbBr<sub>2</sub>, the band gap energy is enhanced, which could be ascribed to the varied structural properties due to composition change.

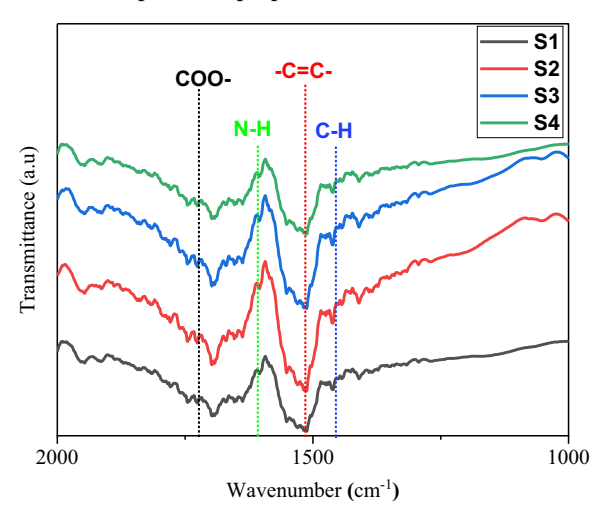
### 3.3. FTIR analysis

The FTIR spectra of the fabricated thin films were recorded between 3000 and 1000 cm<sup>-1</sup>. The FTIR analysis of fabricated thin films is presented in Figure 13, which revealed that the band at 1457 cm<sup>-1</sup> is C-H stretching vibrations in alkenes. The peaks at 1517 cm<sup>-1</sup> are associated with -C=C- stretching vibrations related to the presence of alkenes, and the peaks at 1610 cm<sup>-1</sup> are concerned with N-H stretching vibration due to the presence of

Table 3
Band gap energy values of the CsPbIBr<sub>2</sub> thin films prepared for different PbBr<sub>2</sub> concentration

Sample	Heated (°C)	Band gap (eV)
S1	120	2.23
S2	120	2.21
S3	120	2.20
S4	120	2.24

Figure 13
FTIR spectra of prepared CsPbIBr<sub>2</sub> thin films



primary amines. The bands at 1723 cm<sup>-1</sup> are attributed to COO-stretching vibrations of carbonyl group.

# 3.4. Conductivity determination

There are many methods to determine conductivity type, either n-type or p-type, in a semiconductor material. In this work, conductivity type was determined by applying probe method. A standard multimeter and a soldering iron are used to diagnose that whether a semiconductor is n-type or p-type. The probes connected to the multimeter are placed on the surface of sample.

We heated the positive terminal (anode) of multimeter and kept negative terminal at environmental temperature. In Figure 14, the conductivity determination procedure of all prepared samples is presented; Figure 14(a) is the experimental setup and Figure 14(b) shows the response of prepared thin films. In hot-probe technique, if both probes of voltmeter are placed on the surface of a n-type sample and heated anode probe then multimeter would show a positive response. But when probes are placed on the surface of a p-type sample, then a negative response will be displaced on the panel of multimeter. We observed that the multimeter showed not any noticeable response on heating the anode probe. Only a small fluctuating response was observed around equilibrium. This behavior confirmed the intrinsic nature of prepared of perovskite CsPbIBr2 thin films.

#### 3.5. Thickness measurement

The thin film thickness was estimated by weight difference method where the substrate weight was measured two times: (i) before deposition  $(m_1)$  and (ii) after deposition  $(m_2)$  of thin film on substrate. A precise electronic balance with sensitivity of  $(10^{-6} \text{ g})$  was used to determine the mass difference  $(\Delta m = m_2 - m_1)$ . In this case, it refers to how much film has been applied to a substrate. The following equation can be used to calculate the film thickness:

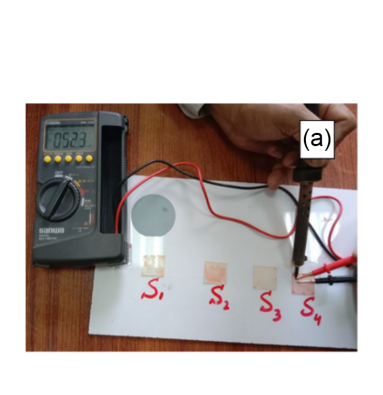
$$t = \frac{\Delta m}{\rho A} \tag{8}$$

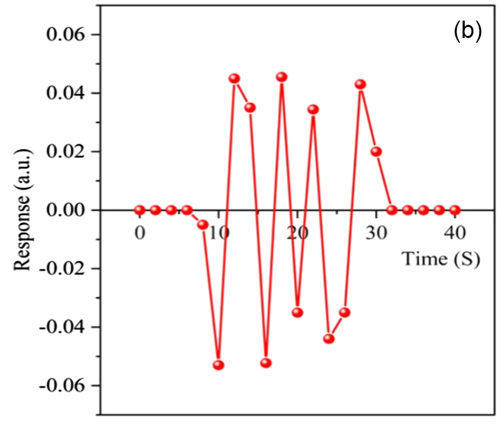
where density  $\rho$  of CsPbIBr<sub>2</sub> thin film is 4.44 g/cm<sup>3</sup>, t is the thickness,  $\Delta m$  is the mass in gm of deposited thin film and A is the area of deposited thin film in cm<sup>2</sup>. All thin films have almost same thickness of 140 nm.

## 4. Conclusion

Thin films of CsPbIBr<sub>2</sub> perovskite materials were deposited on the glass substrates by spin-coating method and then annealed at 120 °C for 20 min to improve their structural properties. The thin films were characterized by their optical parameters, conductivity type and structural properties. The XRD analysis revealed the polycrystalline structure of these thin films, and larger crystallite size was observed for higher concentration ratio CsI:PbBr<sub>2</sub> of 1:1.6. This increase in crystallite size effected other physical properties. The XRD analysis revealed the polycrystalline structure of these

Figure 14
Conductivity type determination: (a) experimental setup, (b) response of prepared thin films





thin films, and larger crystallite size was observed for higher concentration ratio Csl:PbBr<sub>2</sub> of 1:1.6.

# Acknowledgement

This research work is supported by the Higher Education Commission (HEC) of Pakistan. Ghulam Hasnain Tariq acknowledges the HEC of Pakistan for the funding received through NRPU Project No: 10304/Punjab/NRPU/R&D/HEC/2017 and Sana Ullah acknowledges the HEC Pakistan for funding received through NRPU Project No: 20-14709/NRPU/R&D/HEC/2021. Both the authors thankfully appreciate and acknowledge HEC for promoting research environment through project funding schemes.

## **Funding Support**

This research work is supported by the Higher Education Commission (HEC) of Pakistan.

#### **Ethical Statement**

This study does not contain any studies with human or animal subjects performed by any of the authors.

#### **Conflicts of Interest**

The authors declare that they have no conflicts of interest to this work.

## **Data Availability Statement**

Data are available from the corresponding author upon reasonable request.

## **Author Contribution Statement**

S. Jalil: Methodology, Software, Validation, Formal analysis, Investigation, Resources, Data curation, Writing - original draft, Writing – review & editing, Visualization, Project administration. Ghulam Hasnain Tarig: Conceptualization, Software, Validation, Formal analysis, Investigation, Resources, Data curation, Writing - original draft, Writing - review & editing, Visualization, Supervision, Project administration, Funding acquisition. S. Yaseen: Methodology, Software, Validation, Formal analysis, Investigation, Resources, Data curation, Writing - original draft, Writing - review & editing, Visualization. Sana Ullah: Conceptualization, Validation, Formal analysis, Resources, Data curation, Writing – original draft, Visualization, Supervision, Funding acquisition. Muhammad Ijaz Khan: Methodology, Software, Validation, Formal analysis, Writing - original draft, Visualization. Ghulam Asghar: Validation, Formal analysis, Writing - original draft, Visualization.

# References

- [1] Kalsia, M., Sharma, A., Kaushik, R., & Dondapati, R. S. (2023). Evaporative cooling technologies: Conceptual review study. Evergreen: Joint Journal of Novel Carbon Resource Sciences & Green Asia Strategy, 10(1), 421–429. https://doi.org/10.5109/6781102
- [2] Verma, K., Prakash, O., Paikra, A. S., & Tiwari, P. (2023). Photovoltaic panel integration using phase change material (PCM): Review. Evergreen: Joint Journal of Novel Carbon

- Resource Sciences & Green Asia Strategy, 10(1), 444–453. https://doi.org/10.5109/6782147
- [3] Indartono, Y. S., Nur, A. M., Divanto, A., & Adiyani, A. (2023). Design and testing of thermosiphon passive cooling system to increase efficiency of floating photovoltaic array. *Evergreen: Joint Journal of Novel Carbon Resource Sciences & Green Asia Strategy*, 10(1), 480–488. https://doi.org/10.5109/6782151
- [4] Akter, N., Hossion, A., & Amin, N. (2022). Fabrication of oxide passivated and antireflective thin film coated emitter layer in two steps for the application in photovoltaic. *Evergreen: Joint Journal of Novel Carbon Resource Sciences & Green Asia Strategy*, 9(3), 654–661. https://doi.org/10.5109/4842524
- [5] Arifin, Z., Hadi, S., Suyitno, Sutanto, B., & Widhiyanuriyawan, D. (2022). Investigation of curcumin and chlorophyll as mixed natural dyes to improve the performance of dye-sensitized solar cells. Evergreen: Joint Journal of Novel Carbon Resource Sciences & Green Asia Strategy, 9(1), 17–22. https://doi.org/10.5109/4774212
- [6] Jaffar, H. A., Ismaeel, A. A., & Shuraiji, A. L. (2022). Review of hybrid photovoltaic-air updraft solar application: Present and proposed state models. *Evergreen: Joint Journal of Novel Carbon Resource Sciences & Green Asia Strategy*, 9(4), 1181–1202. https://doi.org/10.5109/6625729
- [7] Widhiyanuriyawan, D., Arifin, Z., Muwaffaq, A., Suyitno, S., Hadi, S., Prasetyo, S. D., & Sutanto, B. (2023). The effect of electrospinning precursor flow rate with rotating collector on ZnO nanofiber size results on double-layered DSSC photoanode fabrication. Evergreen: Joint Journal of Novel Carbon Resource Sciences & Green Asia Strategy, 10(1), 504–509. https://doi.org/10.5109/6782154
- [8] Harsito, C., Putra, M. R. A., Purba, D. A., & Triyono, T. (2023). Mini review of thermoelectric and their potential applications as coolant in electric vehicles to improve system efficiency. Evergreen: Joint Journal of Novel Carbon Resource Sciences & Green Asia Strategy, 10(1), 469–479. https://doi.org/10.5109/6782150
- [9] Tan, X., Liu, X., Liu, Z., Sun, B., Li, J., Xi, S., ..., & Liao, G. (2020). Enhancing the optical, morphological and electronic properties of the solution-processed CsPbIBr<sub>2</sub> films by Li doping for efficient carbon-based perovskite solar cells. *Applied Surface Science*, 499, 143990. https://doi.org/10.1016/j.apsusc.2019.143990
- [10] Cao, S., Wang, H., Li, H., Chen, J., & Zang, Z. (2020). Critical role of interface contact modulation in realizing lowtemperature fabrication of efficient and stable CsPbIBr<sub>2</sub> perovskite solar cells. *Chemical Engineering Journal*, 394, 124903. https://doi.org/10.1016/j.cej.2020.124903
- [11] Zhang, W., Zhang, Z., Jiang, Q., Wei, Z., Zhang, Y., You, H., ..., & Zhang, C. (2020). Charge-transporting-layer-free, vacuum-free, all-inorganic CsPbIBr<sub>2</sub> perovskite solar cells via dipoles-adjusted interface. *Nanomaterials*, 10(7), 1324. https://doi.org/10.3390/nano10071324
- [12] Zhu, W., Zhang, Q., Chen, D., Zhang, Z., Lin, Z., Chang, J., ..., & Hao, Y. (2018). Intermolecular exchange boosts efficiency of air-stable, carbon-based all-inorganic planar CsPbIBr<sub>2</sub> perovskite solar cells to over 9%. Advanced Energy Materials, 8(30), 1802080. https://doi.org/10.1002/aenm.201802080
- [13] Yi, C., Luo, J., Meloni, S., Boziki, A., Ashari-Astani, N., Grätzel, C., ..., & Grätzel, M. (2016). Entropic stabilization of mixed A-cation ABX<sub>3</sub> metal halide perovskites for high performance perovskite solar cells. *Energy & Environmental Science*, *9*(2), 656–662. https://doi.org/10.1039/C5EE03255E
- [14] Wang, Y., Dar, M. I., Ono, L. K., Zhang, T., Kan, M., Li, Y., ..., & Zhao, Y. (2019). Thermodynamically stabilized

- β-CsPbI<sub>3</sub>-based perovskite solar cells with efficiencies >18%. *Science*, 365(6453), 591–595. https://doi.org/10.1126/science.aav8680
- [15] Zhu, W., Zhang, Z., Chai, W., Zhang, Q., Chen, D., Lin, Z., ..., & Hao, Y. (2019). Band alignment engineering towards high efficiency carbon-based inorganic planar CsPbIBr<sub>2</sub> perovskite solar cells. *ChemSusChem*, 12(10), 2318–2325. https://doi.org/10.1002/cssc.201900611
- [16] Faridi, A. W., Imran, M., Tariq, G. H., Ullah, S., Noor, S. F., Ansar, S., & Sher, F. (2023). Synthesis and characterization of high-efficiency halide perovskite nanomaterials for lightabsorbing applications. *Industrial & Engineering Chemistry Research*, 62(11), 4494–4502. https://doi.org/10.1021/acs.iecr. 2c00416
- [17] Ou, Q., Bao, X., Zhang, Y., Shao, H., Xing, G., Li, X., ..., & Bao, Q. (2019). Band structure engineering in metal halide perovskite nanostructures for optoelectronic applications. *Nano Materials Science*, *1*(4), 268–287. https://doi.org/10.1016/j.nanoms.2019.10.004
- [18] Erkılıç, U., & Ago, H. (2020). Type-I heterostructure and improved phase stability of formamidinium lead iodide perovskite grown on WS<sub>2</sub>. Evergreen: Joint Journal of Novel Carbon Resource Sciences & Green Asia Strategy, 7(3), 323–328. https://doi.org/10.5109/4068610
- [19] Luo, Z., Zhang, C., Yang, L., & Zhang, J. (2022). Ambient spray coating of organic-inorganic composite thin films for perovskite solar cell encapsulation. *ChemSusChem*, 15(3), e202102008. https://doi.org/10.1002/cssc.202102008
- [20] Liu, K., Fong, P. W. K., Liang, Q., & Li, G. (2021). Upscaling perovskite solar cells via the ambient deposition of perovskite thin films. *Trends in Chemistry*, 3(9), 747–764. https://doi.org/ 10.1016/j.trechm.2021.06.003
- [21] Zhang, Z., Bao, C., Yao, W., Ma, S., Zhang, L., & Hou, S. (2011). Influence of deposition temperature on the crystallinity of AI-doped ZnO thin films at glass substrates prepared by RF magnetron sputtering method. *Superlattices and Microstructures*, 49(6), 644–653. https://doi.org/10.1016/j.spmi.2011.04.002
- [22] Kim, G. H., Shin, H. S., Ahn, B. D., Kim, K. H., Park, W. J., & Kim, H. J. (2009). Formation mechanism of solution-processed nanocrystalline InGaZnO thin film as active channel layer in thin-film transistor. *Journal of the Electrochemical society*, 156(1), H7. https://doi.org/10.1149/1.2976027
- [23] Mi, Y., Wang, J., Yang, Z., Wang, Z., Wang, H., & Yang, S. (2014). A simple one-step solution deposition process for constructing high-performance amorphous zirconium oxide thin film. RSC Advances, 4(12), 6060–6067. https://doi.org/ 10.1039/C3RA46169F
- [24] He, W., Hu, J., Chen, C., Chen, Y., Zeng, L., Zhang, X., ..., & Guo, F. (2020). Temperature-assisted crystal growth of photovoltaic α-phase FAPbI<sub>3</sub> thin films by sequential blade coating. *ACS Applied Materials & Interfaces*, 12(50), 55830–55837. https://doi.org/10.1021/acsami.0c15733
- [25] Cao, X., Zhang, G., Hao, L., Ding, X., Dong, T., Li, X., ..., & Wei, J. (2022). Achieving one-step solution deposition of high quality CsPbBr<sub>3</sub> films for efficient solar cells through halide ion exchange. *Journal of Alloys and Compounds*, 919, 165722. https://doi.org/10.1016/j.jallcom.2022.165722
- [26] Feng, M., Feng, R., Pan, Y., Li, R., Yang, R., & Gong, B. (2022). Preparation of Si thin films on copper foil using pulse current electrodeposition. *Materials Letters*, 324, 132793. https://doi.org/10.1016/j.matlet.2022.132793

- [27] Hasaneen, M. F., Shalaby, M. S., Yousif, N. M., Diab, A. K., & El Agammy, E. F. (2022). Structural and optical properties of transparent conducting oxide Cd<sub>1-x</sub>Cr<sub>x</sub>O thin films prepared by the sol-gel dip-coating method. *Materials Science and Engineering: B*, 280, 115703. https://doi.org/10.1016/j.mseb. 2022.115703
- [28] El Radaf, I. M., & Al-Zahrani, H. Y. S. (2022). Structural and optical studies of the novel BiSbS<sub>3</sub> thin films prepared by chemical bath deposition technique. *Physica B: Condensed Matter*, 631, 413655. https://doi.org/10.1016/j.physb.2021.413655
- [29] Dastan, D., Panahi, S. L., & Chaure, N. B. (2016). Characterization of titania thin films grown by dip-coating technique. *Journal of Materials Science: Materials in Electronics*, 27(12), 12291–12296. https://doi.org/10.1007/ s10854-016-4985-4
- [30] Mohammed, M. A., Abdulridha, W. M., & Abd, A. N. (2018). Thickness effect on some physical properties of the Ag thin films prepared by thermal evaporation technique. *Journal of Global Pharma Technology*, 10(3), 613–619.
- [31] Beard, E. J., & Cole, J. M. (2022). Perovskite- and dyesensitized solar-cell device databases auto-generated using chemdataextractor. *Scientific Data*, 9(1), 329. https://doi.org/ 10.1038/s41597-022-01355-w
- [32] Mishra, R., Doda, D. K., Jangid, S., & Kumar, S. (2023). Review on solar hybrid systems and its approaches for green power generation. *IOP Conference Series: Earth and Environmental Science*, 1279(1), 012007. https://doi.org/10.1088/1755-1315/1279/1/012007
- [33] Gunawan, Y., Nurliyanti, V., Akhiriyanto, N., Kasbi, S., Ahadi, K., Sujono, ..., & Permana, M. R. F. (2022). A comparative study of photovoltaic water pumping system driving conventional AC single-phase and three-phase motor submersible pumps. Evergreen: Joint Journal of Novel Carbon Resource Sciences & Green Asia Strategy, 9(3), 893–902. https://doi.org/10.5109/4843121
- [34] Imran, M., Asghar, G., Tariq, G. H., Waseem Faridi, A., Bano, S., Shehzad Shifa, M., & Ullah, S. (2023). Investigation of annealing effects on physical properties of chemically prepared copper oxide thin films. *Results in Optics*, 10, 100331. https://doi.org/10.1016/j.rio.2022.100331
- [35] Shah, M. S., Ullah, S., Tariq, G. H., Sahar, M. S. U., Asghar, G., & Anis-ur-Rehman, M. (2022). Thickness-dependent physical properties of tin sulfide thin films for an efficient sunlight-absorbing layer. *Journal of Electronic Materials*, 51(11), 6454–6462. https://doi.org/10.1007/s11664-022-09881-4
- [36] Guo, Y., Yin, X., Liu, J., & Que, W. (2019). Highly efficient CsPbIBr<sub>2</sub> perovskite solar cells with efficiency over 9.8% fabricated using a preheating-assisted spin-coating method. *Journal of Materials Chemistry A*, 7(32), 19008–19016. https://doi.org/10.1039/C9TA03336J
- [37] Lin, J., Lai, M., Dou, L., Kley, C. S., Chen, H., Peng, F., ..., & Yang, P. (2018). Thermochromic halide perovskite solar cells. *Nature Materials*, *17*(3), 261–267. https://doi.org/10.1038/s41563-017-0006-0
- [38] Wang, D., Li, W., Liu, X., Li, G., Zhang, L., Li, R., ..., & Lan, Z. (2021). Carbon-based stable CsPbIBr<sub>2</sub> solar cells with efficiency of over 10% from bifunctional quinoline sulfate modification. ACS Applied Energy Materials, 4(6), 5747–5755. https://doi.org/10.1021/acsaem.1c00575
- [39] Wang, H., Cao, S., Yang, B., Li, H., Wang, M., Hu, X., ..., & Zang, Z. (2020). NH<sub>4</sub>Cl-modified ZnO for high-performance CsPbIBr<sub>2</sub> perovskite solar cells via low-temperature process.

- Solar RRL, 4(1), 1900363. https://doi.org/10.1002/solr. 201900363
- [40] Henry, J., Daniel, T., Balasubramanian, V., Mohanraj, K., & Sivakumar, G. (2022). Chemically deposited p-type MoBiCuS<sub>4</sub> thin film for photoelectrochemical cell applications. *Phosphorus, Sulfur, and Silicon and the Related Elements*, 197(3), 152–157. https://doi.org/10.1080/10426507.2021.1990921
- [41] Chin, S. H., Cortecchia, D., Forzatti, M., Wu, C. S., Alvarado-Leaños, A. L., Folpini, G., ..., & Bolink, H. J. (2024). Stabilizing single-source evaporated perovskites with organic interlayers for amplified spontaneous emission. *Advanced Optical Materials*, 12(13), 2302701. https://doi.org/10.1002/adom.202302701
- [42] Hariech, S., Aida, M. S., Bougdira, J., Belmahi, M., Medjahdi, G., Genève, D., ..., & Rinnert, H. (2018). Cadmium sulfide thin films growth by chemical bath deposition. *Journal of Semiconductors*, 39(3), 034004. https://doi.org/10.1088/1674-4926/39/3/034004
- [43] Atuchin, V. V., Isaenko, L. I., Kesler, V. G., Lin, Z. S., Molokeev, M. S., Yelisseyev, A. P., & Zhurkov, S. A. (2012). Exploration on anion ordering, optical properties and electronic structure in K<sub>3</sub>WO<sub>3</sub>F<sub>3</sub> elpasolite. *Journal of Solid*

- State Chemistry, 187, 159–164. https://doi.org/10.1016/j.jssc. 2011.12.037
- [44] Reshak, A. H., Alahmed, Z. A., Bila, J., Atuchin, V. V., Bazarov, B. G., Chimitova, O. D., ..., & Yelisseyev, A. P. (2016). Exploration of the electronic structure of monoclinic α-Eu<sub>2</sub>(MoO<sub>4</sub>)<sub>3</sub>: DFT-based study and X-ray photoelectron spectroscopy. *The Journal of Physical Chemistry C*, 120(19), 10559–10568. https://doi.org/10.1021/acs.jpcc.6b01489
- [45] Azarapin, N. O., Aleksandrovsky, A. S., Atuchin, V. V., Gavrilova, T. A., Krylov, A. S., Molokeev, M. S., ..., & Andreev, O. V. (2020). Synthesis, structural and spectroscopic properties of orthorhombic compounds BaLnCuS<sub>3</sub> (Ln = Pr, Sm). *Journal of Alloys and Compounds*, 832, 153134. https://doi.org/10.1016/j.jallcom. 2019.153134

**How to Cite:** Jalil, S., Tariq, G. H., Yaseen, S., Ullah, S., Khan, M. I., & Asghar, G. (2025). Study of the Effects of Compositional Constituents on the Physical Properties of Inorganic Halide Perovskite Thin Films Prepared via Spin-Coating Deposition Method. *Journal of Optics and Photonics Research*, *2*(4), 212–221. https://doi.org/10.47852/bonviewJOPR52024061